# Survey on damage mechanics models for fatigue life prediction

S. Silitonga [1, 2, 3], J. Maljaars [2], F. Soetens [3] and H.H. Snijder [3]

[1] Materials innovation institute (M2i), Delft, the Netherlands

[2] TNO, Structural Reliability, Delft, the Netherlands

[3] Eindhoven University of Technology, Department of the Built Environment, Eindhoven, the Netherlands

**Engineering methods to predict the fatigue life of structures have been available since the beginning of the 20th century. However, a practical problem arises from complex loading conditions and a significant concern is the accuracy of the methods under variable amplitude loading. This paper provides an overview of existing fatigue damage models with emphasis on relatively new alternative models and computational strategies to predict fatigue life. These models are compared and promising new capabilities are discussed.**

*Key words: Continuum damage mechanics, fatigue damage, cohesive zone*

## 1    Introduction

Fatigue failure is an important mode of mechanical failure in the field of engineering. This type of failure was recognized first by August Wöhler in the 1850 [Schütz, 1996] who published his fatigue test results of railway axles in 1870 [Wöhler, 1870]. He found that application of a single load far below the static strength of a structure did not cause damage but repetition of the same load could induce complete failure.

Fatigue is featured by the following main characteristic processes: repeated loading may cause nucleation of small crack(s), followed by the growth of a dominant crack which may finally lead to complete fracture after a sufficient number of load repetitions.

This paper provides an overview of fatigue damage models and computational strategies to predict fatigue life, emphasis is on two relatively new and unknown strategies from the point of view of the engineer. The paper is organized in the following manner: Section 2 consists of an overview of the basics of fatigue, in this section the physical phenomena of fatigue damage are explored. Subsequently, the current fatigue design approaches applied

in engineering are revisited, namely the total life approach (infinite-life and safe-life method) and the damage tolerant approach based on Linear Elastic Fracture Mechanics (LEFM).

Based on its promising characteristics to model fatigue damage, a relatively new field called Continuum Damage Mechanics (CDM) is elaborated in Section 3. It begins with a presentation of the fundamental concept and definitions. In addition, a brief description on how the CDM approach is able to represent physical damage through a mathematical formulation in order to accurately describe the damage evolution is given. Section 3 also includes the most common method to quantify the damage in experiments.

The paper continues with a review on existing fatigue damage models based on CDM. There are four fatigue damage models studied in this paper, each model contains a unique strategy to describe fatigue damage. Section 4 begins with a general description of these models along with their related physical background. Each model contains several specific parameters to describe, especially, the damage evolution function. These parameters are generally determined from standard material tests.

Section 5 presents a discontinuous damage model. This damage model is based on a cohesive zone model where the fatigue damage mechanism is implemented into the cohesive law to describe fatigue damage. The section begins with the basic concept of cohesive zone theory and this is followed by the description of the damage mechanism.

The final section of the paper – Section 6 – consists of conclusions and comments on previous sections. It describes limitations and advantages as well as opportunities for improvements to obtain a model that better fits the results of fatigue experiments as compared to the current state of the art.

## 2    Fatigue

According to the ASTM definition, fatigue is a process of *progressive localized permanent* structural change occurring in a material subjected to conditions that produce *fluctuating stresses* and strains at a point or some points and that may culminate in *cracks* or complete *fracture* after a sufficient number of fluctuations [ASTM, 2002]. The fluctuating stress and strain described above are primarily due to mechanical loading which in turn governs the nucleation and propagation of the crack. However, several other factors such as temperature and chemical environment can affect the behaviour of these phenomena. These effects are not considered in this work. Furthermore, the focus is on fatigue of metal alloys.

## 2.1 Fatigue mechanisms

The fatigue process is divided into three distinct stages. In the first stage, a microcrack nucleates at one, or sometimes at several locations in the material. Subsequently, a main crack (macrocrack) grows in a stable manner during cyclic loading. Finally, when it has reached a critical size, the crack becomes unstable and sudden fracture occurs, usually within one or a few cycles. In most cases, these stages can be identified afterwards on the fracture surface.

### 2.1.1 Cyclic characteristic

Cyclic loading is an idealization of the fluctuating loads that are applied to structures. This can be a periodical stress or strain with a certain frequency, mean value and amplitude together with the wave shape (sinusoidal, triangular etc.). Standard terminology used for constant amplitude fatigue loading is shown in Figure 1. Another important definition often used in constant amplitude fatigue loading is the load ratio ($R = \sigma_{min}/\sigma_{max}$). Fatigue damage depends primarily on the stress amplitude. A high stress amplitude leads to a short fatigue life and vice versa. Cycles with a high mean stress lead to a shorter fatigue life than cycles with the same amplitude but with a lower mean stress. However, in welded connections, the stress range is considered the most relevant as the effect of the applied mean stress is locally compromised by the presence of residual stresses.

Under laboratory conditions, the fatigue life of metals is fairly independent of the cycle shape and frequency. However, viscous effects generated by hysteretic heating becomes important in a very high loading frequency.
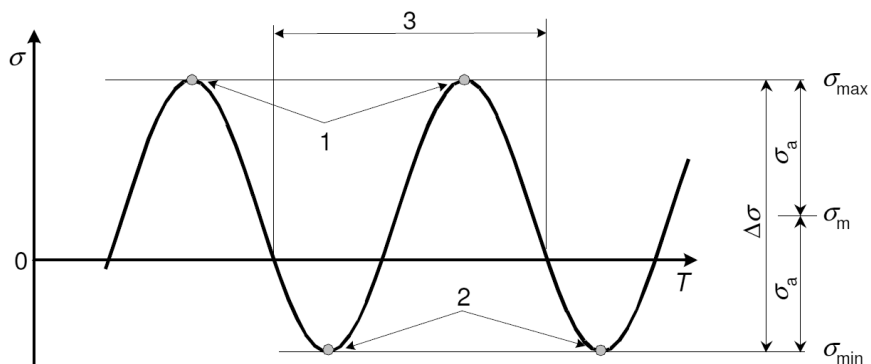


Figure 1. Terminology relating to cyclic loading: 1 - stress peak; 2 - stress valley; 3 - stress cycle; $\sigma_{max}$ - maximum stress; $\sigma_{min}$ - minimum stress; $\sigma_m$ - mean stress; $\sigma_a$ - stress amplitude; $\Delta_s$ - stress range
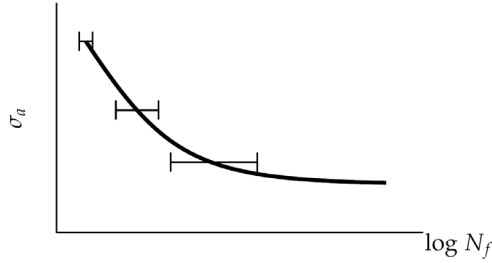
*Figure 2. Typical presentation of an S-N Curve; larger scatter with smaller applied loads*

The Wöhler curve or S-N curve presents the results of fatigue tests. It plots the stress range $\Delta_s$ (or stress amplitude $\sigma_a$) with certain load ratio against the number of cycles at failure (fatigue life $N_f$) in a semi or double logarithmic scale. Figure 2 shows a typical S-N curve, at low stress level, the curve shows an asymptotic behaviour which describes a fatigue property called the fatigue limit. The fatigue limit is the cyclic stress level below which no fatigue failure is expected.
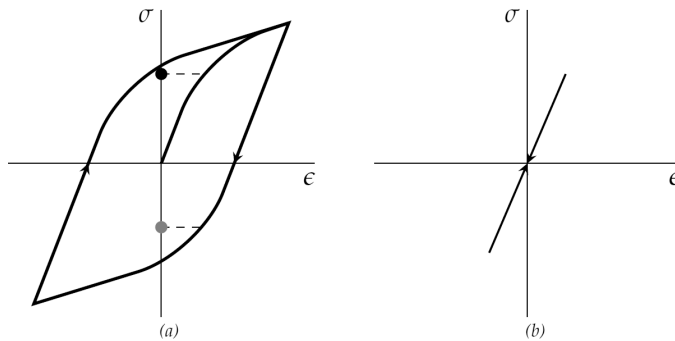


*Figure 3. Schematic stress-strain response of cyclic loading: (a) LCF (•$= \sigma_y^+$ and •$= \sigma_y^-$) (b) HCF*

The short-life region of the S-N curve is referred to as the low cycle fatigue (LCF) region. The region is identified by dominant plastic yielding in subsequent opposite direction, which leads to a very short fatigue life. The term high cycle fatigue (HCF) is used to describe the large fatigue life of materials which is shown in the region of stress levels that do not result in yielding in opposite direction. The difference in stress-strain response between LCF and HCF is schematically illustrated in Figure 3.

In engineering practice, HCF corresponds to a number of cycles greater than $10^5$ [Lemaitre & Desmorat, 2005]. A physically based definition often used to refer to high/low cycle fatigue is the amount of macroplastic strain compared to the elastic strain. HCF

28

corresponds to a very small macroplastic strain and vice versa. The plastic deformation is not present in the graph, however, behaviour similar to that in low cycle fatigue is expected in microscale. At a very large number of cycles (approx. $N > 10^8$), the fatigue failure mode changes from a surface crack to a subsurface crack. This manifests as a change in the slope of the S-N curve for constant amplitude loading. Note that the common consensus of a fatigue limit after a large-enough number of cycles is enfeebled by tests in the giga-cycle range [Stanzl-Tschegg & Mayer, 2001]. This paper emphasizes on HCF of surface cracks, i.e. $10^5 < N < 10^8$.

In HCF, normal mean stresses have a significant effect on the fatigue behaviour of components except for welded structures where high residual stresses are present. Normal mean stresses are responsible for the opening and closing state of micro-cracks. The opening of micro-cracks accelerates the rate of crack propagation and micro-cracks closure will slow down the growth of cracks. Thus, tensile normal mean stresses are detrimental and compressive normal mean stresses are less detrimental. The shear mean stress does not influence the opening and closing state of micro-cracks, and therefore, has little effect on crack propagation. There is very little or no effect of mean stress on fatigue strength in the LCF region in which the large amounts of plastic deformation cancel out any beneficial or detrimental effect of a mean stress.

### 2.1.2 Crack initiation

Crack initiation is a consequence of cyclic slip, i.e. cyclic plastic deformation as a result of moving dislocations which is usually limited to a small number of grains. This phenomenon, so-called microplasticity, preferably occurs in grains at the material surface where constraint on slip due to the surrounding material exists on one side only. A general situation in which nucleation occurs due to slip under cyclic loading is shown in Figure 4(a). It shows progressive development of an extrusion/intrusion pair, often called (persistent) slip band. The pairs of extrusion/intrusion act as micro-notches that create stress concentrations which in turn promote additional slips growing deeper inside the material and eventually develop into a (micro-)crack.

Fatigue crack initiation is primarily a surface phenomenon. However, not all fatigue cracks nucleate along slip bands, fatigue cracks may nucleate at or near material discontinuities or sometimes just below the metal surface. These discontinuities include inclusions, second-phase particles, corrosion pits, grain boundaries, twin boundaries, pores and voids. Microcracks can also be present in metals prior to any cyclic loading due to manufacturing
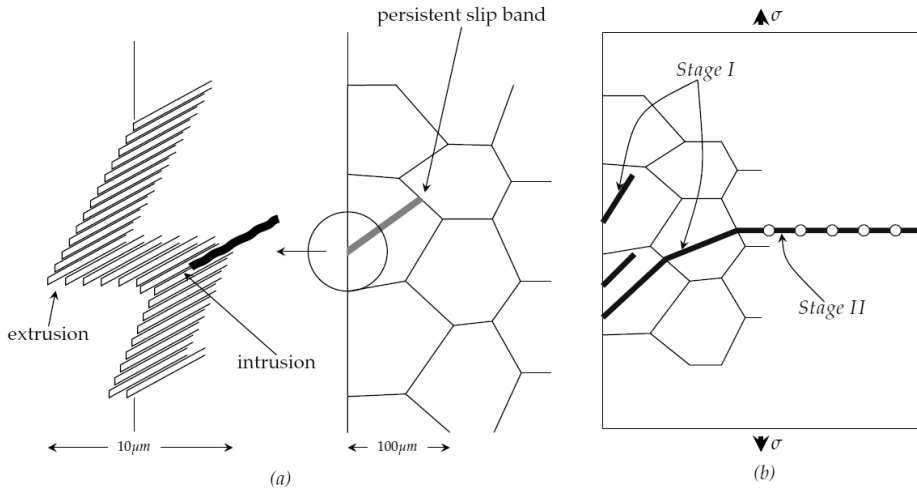
*Figure 4. (a) Schematic presentation of (a) crack initiation in persistent slip bands and (b) crack growth in mode I loading*

processes and treatments such as welding. Thus, in some cases, the nucleation phase of fatigue can be non-existing or very short.

An accepted definition of the end of the crack initiation is non-existing. In engineering practice, it is, sometimes, defined as the detection threshold of a specific detection technique utilized. In this definition, the crack initiation phase depends on the accuracy of the method. An alternative, more consistent definition of crack initiation is a microcrack that reaches the grain size of the material.

### 2.1.3 Crack propagation

Once microcracks are present and cyclic loading continues, fatigue cracks tend to coalesce and grow along the plane of maximum tensile stress. Fatigue crack growth usually consists of two subsequent stages, being growth in a shear mode (stage I) followed by growth in a tension mode (stage II) (Figure 4(b)).

The stage I growth is small, usually of the order of several grains. Stage II crack growth in ductile materials often occupies a large fraction of the fracture surface (Figure 6). In many metal alloys, Stage II crack growth is visible at the cracked surface by striations. They are formed by alternate blunting and sharpening of the crack tip in the tensile and compressive portions of the loading cycle (shown in Figure 5). In many studies, at moderate to high load level, each striation has been shown to correspond to one load cycle. In HCF, in an ideally smooth component, the crack initiation phase occupies most of its

30

fatigue life; it may constitute more than 80% of the total fatigue life. This is not the case if material and geometrical imperfections are present. In many cases initial microcracks have already developed during manufacturing (e.g. machining and welding). In such cases, the fatigue life is dominated by the crack growth phase.
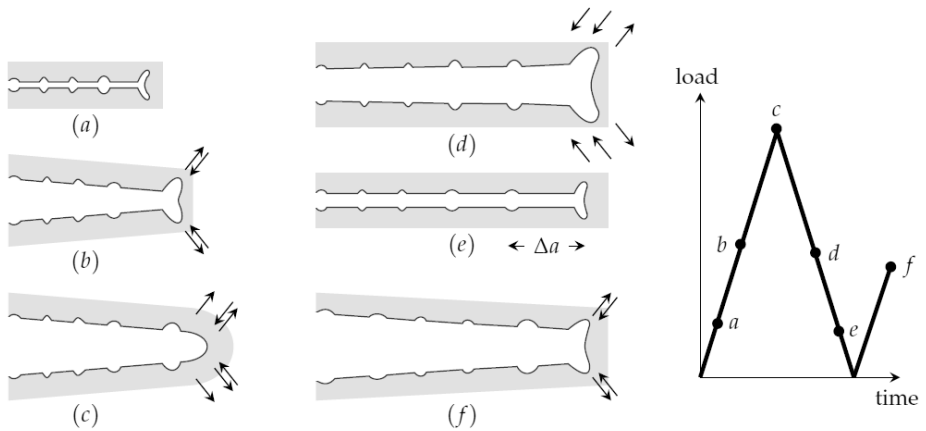


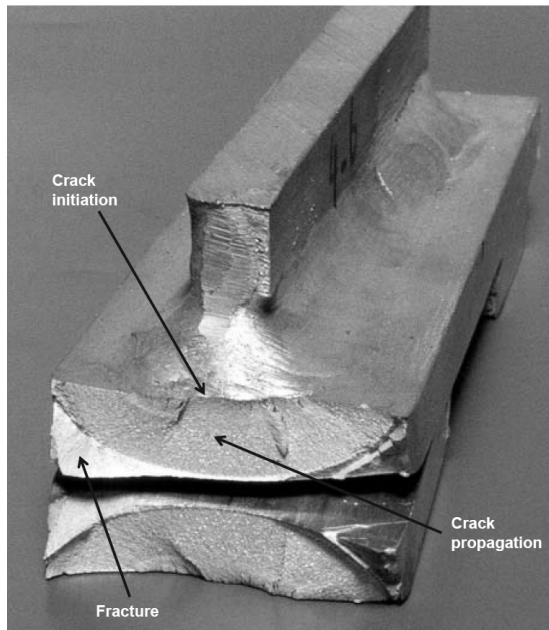*Figure 5. Schematic presentation of crack tip plastic blunting and sharpening*



*Figure 6. Fracture surface of welded alloy specimen*

### 2.1.4 Fracture

After a sufficient number of cycles, the crack reaches a critical size at which the crack becomes unstable. The remaining cross section is traversed by dynamic fracture, usually within one or a few cycles. This critical condition in practice is commonly governed by a fracture mechanics criterion. The corresponding fracture surface is usually rougher than the crack surface caused by stage II fatigue (Figure 6). Its size may vary from a small fraction of the cross section for ductile materials at low stress level to almost the entire area for brittle materials at high stress level. The specific fracture mode by which final fracture occurs depends on the material ductility, stress state level and frequency.

## 2.2 Engineering fatigue design

The fatigue failure criterion plays an important role in the design of many structural applications. From the time of Wöhler, works to resolve fatigue have produced numerous strategies, diagram types, empirical relations, rules of thumb, etc., in designing against fatigue. The two popular strategies to predict the fatigue life, i.e. total-life design and defect-tolerant design, are subsequently elaborated in this subsection.

### 2.2.1 Total life approach

As the name suggests this approach makes no distinction between the crack initiation and the propagation phases. The most common fatigue design based on this approach is the stress-based method. Predicting the fatigue life using this method is conducted by means of a 'similitude concept'. It allows engineers to relate the behaviour of small-scale test specimens defined under carefully controlled conditions with the likely performance of real structures subjected to variable or constant amplitude loads (VAL or CAL) under either simulated or actual service conditions.

The S-N curve, defined in the previous section, is the core of this method in designing structural components against fatigue. Many standards use the concept of the S-N curve as fatigue design procedure. A typical S-N curve plotted in log-log scale can be approximated, especially the HCF region, by a fairly linear relationship [Basquin, 1910],

$$\sigma_a = \frac{\Delta\sigma}{2} = S'_f (N_f)^b \tag{1}$$

where $S'_f$ is the fatigue strength coefficient, $b$ is known as the fatigue strength exponent or Basquin exponent and $N_f$ is the number of cycles at failure.

The material S-N curve provides the baseline fatigue data for a given geometry, loading

condition, and material processing. The data can be adjusted, in many cases, to account for realistic component conditions such as notches, size, global geometry, surface finish, surface treatments, temperature, and various types of loading.

Figure 7 shows the typical S-N curve used in EN1999-1-3 (Eurocode 9) for aluminium alloys. The S-N curve derived from standard specimens can be constructed as a piecewise-continuous curve consisting of three distinct linear regions when plotted on log-log scales. The reference fatigue strength ($\Delta\sigma_C$ assumed to be at number of cycles $N_C = 2.106$), constant amplitude fatigue limit ($\Delta\sigma_D$ assumed to be at $N_D = 5.106$ with inverse slope $m_1$) and the cut-off limit or run-out (at $N_L = 108$ with inverse slope $m_2$) are indicated in the curve. A different definition is given by the International Institute of Welding (IIW) for the constant amplitude fatigue limit ($N_{CI\,IIW} = 107$) and IIW omits the constant cut-off limit allowing for declining of the fatigue resistance with a slope of $m_{I\,IIW} = 22$.

### 2.2.2 Damage-tolerant approach

The main difference between damage-tolerant design and the total life approach is the assumption of the existence of a crack at the start of the analysis. The method mainly focuses on the (stable) crack growth period described in Section 2.1.3. In addition, contrary to the empirical S-N methods, this approach is supported by the theory of LEFM. The basis of the damage-tolerant method is the existence of a relationship between the
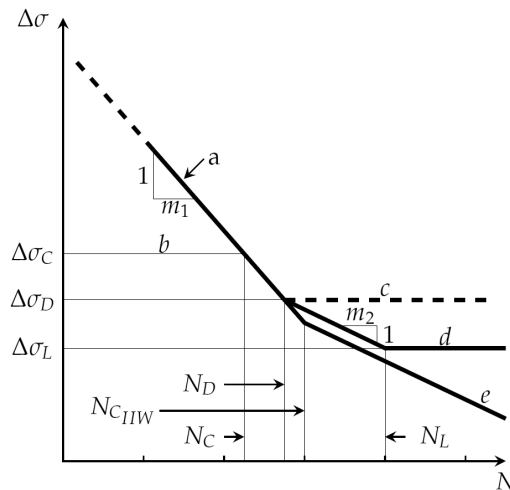


*Figure 7. Fatigue strength curve log-log coordinates; a - fatigue strength ; b - reference fatigue strength; c - constant amplitude fatigue limit; d - cut-off limit; e - IIW declining fatigue resistance*

crack growth rate da/dN and the stress intensity range ($\Delta K = K_{max} - K_{min}$) which may be obtained from experiments. Where a represents the crack size and the maximum and minimum stress intensity factors ($K_{max}$, $K_{min}$), based on LEFM, describe the stress state at the crack tip under the far-field (mode I) stresses $\sigma_{max}$ and $\sigma_{min}$, respectively [Griffith, 1921]. This material-dependent relationship (shown in Figure 8) shows an increase of crack growth rate with increasing stress intensity range. For low values of $\Delta K$, a steep decrease in crack growth rate with decreasing $\Delta K$ is observed. No or hardly any crack growth is expected at a certain value of $\Delta K$, which is called the stress intensity range threshold value, $\Delta K_{th}$. At the other extreme, a rapid increase of da/dN with increasing $\Delta K$ is observed, when the maximum stress intensity approaches the critical stress intensity factor, $K_{Ic}$ or material toughness, $K_{mat}$.
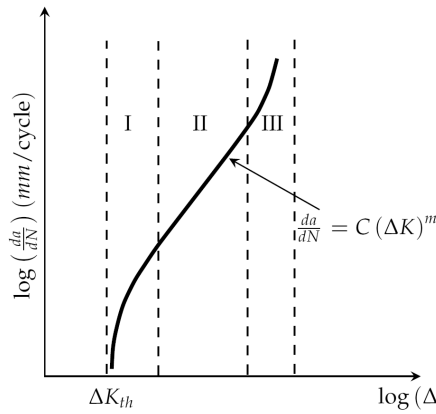


*Figure 8. Crack growth rate da/dN schematically plotted as a function of the stress intensity factor range $\Delta K$ in a log-log scale*

The prediction of (extended) fatigue life, in this case, entails a semi-empirical crack propagation law based on fracture mechanics. This is an approximation of the crack growth rate curve given in Figure 8 which was introduced by Paris [Paris & Erdogan, 1963] therefore also called Paris law,

$$\frac{da}{dN} = C(\Delta K)^m \tag{2}$$

with $C$ and $m$ being the material constants. The fatigue life can be determined by substituting the appropriate expression for $\Delta K$ (dependent on dimension, local geometry and loading type) for a specific structural configuration and integrating the corresponding equation from the initial crack $a_i$ to the critical crack size $a_f$ as follows,

34

$$N_f = \int\limits_{ai}^{af} \frac{1}{C(\Delta K)^m}\, da \qquad\qquad (3)$$

A number of modifications to the Paris law have been proposed over the years to also account for the stress ratio effect [Forman, 1972;Walker, 1970], the threshold limit [McEvily, 1973], large-scale yielding [Dowling & Begley, 1976], crack retardation [Wheeler, 1972; Willenborg *et al.*, 1971] and plasticity-induced crack closure [Elber, 1971; Huang *et al.*, 2005; Newman, 1984]. Despite the extensive use of these models, the essential physical background of fatigue crack growth is not completely described by the theory.

It is important to note that the relation between da/dN and $\Delta K$ is meaningful only if a linear elastic fracture mechanics description is satisfied, i.e. the size of the plastic zone near the crack tip should be much smaller than any relevant length dimensions for the crack problem of interest. In this way, the stress intensity factor controls the plastic deformation near the crack tip, and, in turn, the fracture process near the crack tip. Moreover, the Paris law is not suited to describe small crack growth due to the fact that growth of these small flaws is dominated by microstructural effects. Despite these shortcomings, the method is very useful to determine the (residual) fatigue life in engineering practice.

### 2.2.3 *Complex loading*

Many typical structural components are subjected to cyclic loads during service lives. These loads are often multiaxial in nature with fluctuating amplitudes, mean values and frequencies. Loads that are multiaxial in nature occur when a structural component is simultaneously subjected to tensile (or bending) and torsion loads. If the frequencies of these load types are in-phase, they are called proportional loading. Non-proportional loading is referred if loads are multiaxial with out-of-phase frequencies which lead to a shorter fatigue life. During crack growth, multiaxial loading leads to a mixed-mode state of stress (any combination of the modes shown in Figure 9) at the crack tip which may significantly influence the crack growth direction as well as the crack growth rate.

Varying load amplitude can greatly affect the fatigue life of a component. Application of (single/periodic) overloads during the crack initiation period may result in premature crack initiation which leads to a shorter fatigue life. However, if the overloads are applied during the crack propagation period, crack retardation is expected. This crack retardation is related to the residual compressive stress field induced at the vicinity of the crack tip after an overload. Following an overload, the crack growth driving force is reduced due to
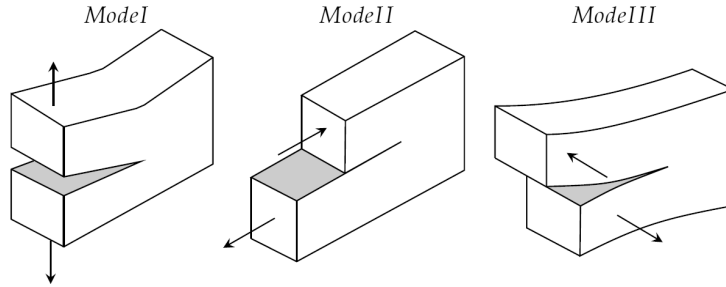
*Figure 9. The three modes of crack tip deformation*

the residual compressive stress, thus retarding the crack propagation. After the crack tip exits the compressive zone, the crack growth rate resumes its original value.

In engineering methods, VAL is usually translated into several blocks of CALs using rain flow analysis. This translation process, however, cannot naturally account for the complex loading effects described previously. A physically based approach should be pursued in order to naturally include the VAL effects on the fatigue life and to provide better results in predicting the fatigue behaviour. Moreover, the crack initiation model should involve microscale phenomena of plasticity and the crack growth model should incorporate crack-tip plasticity to better describe its blunting and sharpening mechanisms during opening of a new crack surface.

## 3    Continuum damage mechanics

The fatigue design methods described previously are, to a certain extent, lacking a theoretical or physical background. Thus, an alternative approach based on damage mechanics is explored in this chapter. The concept of damage was first introduced by Kachanov in 1958 to predict creep failure of metals [Kachanov, 1958]. In 1978, Lemaitre and Chaboche [Lemaitre & Chaboche, 1978], developed the concepts of material damage and established a new branch of mechanics by means of the theory of continuum mechanics. This new theory is called Continuum Damage Mechanics (CDM). This field has developed significantly, especially in the last thirty years, to model other various modes of failure in materials such as ductile damage [Gurson, 1977; Lemaitre, 1985], creep-fatigue interaction [Lemaitre & Chaboche, 1974], LCF in metals [Chow &Wei, 1991; Lemaitre & Desmorat, 2005] and HCF [Lemaitre & Desmorat, 2005; Lemaitre & Doghri, 1994; Lemaitre *et al.*, 1999]. This section provides a general description of CDM, Section 4 describes the application of CDM to fatigue.

36

CDM describes the development of cracks, voids or cavities in each scale that lead to deterioration of the mechanical properties of the materials [Krajcinovic, 1984; Lemaitre & Chaboche, 1978; Murakami, 1983]. Damage in solid materials can be characterized on three scales: the micro, the meso and the macro scale. The microscale is the scale where microvoids, microcracks or decohesion in microstructures are analyzed. Visible or near-visible discrete damage manifestations such as the isolated cracks discussed in fracture mechanics, are treated as phenomena on the macroscale. The mesoscale is a building block of CDM in which discrete phenomena can be smeared into average effects [Cauvin & Testa, 1999].

Models have been developed in recent years to formulate and represent damage on the mesoscale. The method discussed in this chapter is a phenomenological approach, which treats a damaged material element with certain properties as if it were in a homogeneous medium regardless to how those properties physically are affected by damage.

### 3.1    *Representative Volume Element*

As mentioned previously, in the phenomenological approach, CDM divides the material into small elements with homogeneous properties. Such an element is called a representative volume element (RVE). An RVE is the smallest volume of mesoscale in a body where the following conditions are satisfied: the material structural discontinuities can be assumed to be statistically homogeneous and the corresponding mechanical state of the material can be represented by the statistical average of the mechanical variables in that volume [Hashin, 1983; Hill, 1963]. Through the RVE, a material with discontinuous microstructure can be idealized as a continuum by means of the statistical average of the mechanical state in the material. The mechanical state of the continuum is unique only if the RVE is large enough to contain a sufficient number of discontinuities and at the same time small enough so that the variation of the macroscopic variable is insignificantly small [Murakami, 2012].

The size requirement of an RVE depends on the microstructure of the relevant material and on the mechanical phenomena to be considered. For metals, the appropriate RVE size is usually in the order of $(0.1 \text{ mm})^3$ [Lemaitre, 1996]. Among damage phenomena, brittle damage and fatigue damage are much more localized than creep damage and ductile damage. Thus, the required size of an RVE for brittle and fatigue damage is larger than that for creep and ductile damage [Murakami, 2012] such that the localized brittle and fatigue damages can be sufficiently contained in the RVE.

In the phenomenological approach, the discrete entities of damage are not described

explicitly in the RVE, but their combined effects are represented by means of macroscopic internal variables (e.g. plastic strain), in such a way that the formulation of damage can be consistently based on the thermodynamics principles.

## 3.2    *Damage variable*

The damage variable represents the average material degradation within the RVE. It reflects the various types of damage at the micro-scale level such as nucleation and growth of voids, cracks, cavities, micro-cracks, and other microlevel defects [Budiansky & O'connell, 1976; Krajcinovic, 1996; Lubarda & Krajcinovic, 1993]. The choice of the damage variables is an important step in the development of damage models in order to efficiently describe the damage evolution. In the most general three dimensional problem, microcavities, interface debonds and microcrack orientations are most often governed by the loading principle direction and material status (anisotropic or isotropic). Hence, a tensorial variable is more suitable to describe the directional nature of the damage. The most general tensorial damage variable at any given state of damaged material is the eighth-order damage tensor which provides a linear relationship between the elastic moduli of damaged and undamaged material. However, application of this damage tensor in a damage model is difficult in practical situations.

### 3.2.1  *Scalar damage variable*

The damage variable can be defined as the surface density of microcracks and microcavities lying on the plane cutting the RVE (shown in Figure 10(a)). The damage is thus defined as,

$$D = \frac{\delta S_D}{\delta S} \tag{4}$$

where $\delta S$ is the area of the intersection of the plane in the RVE and $\delta S_D$ is the effective area of the intersection of all microcracks or microvoids in that plane in the RVE.

An important concept in CDM is the *effective stress* [Kachanov, 1958; Rabotnov, 1968], it represents the increase of stress $\sigma$ induced by the external loading $F$ due to decrease in the load-carrying area $\tilde{S}$ as illustrated in Figure 10(b). The effective stress is defined as,

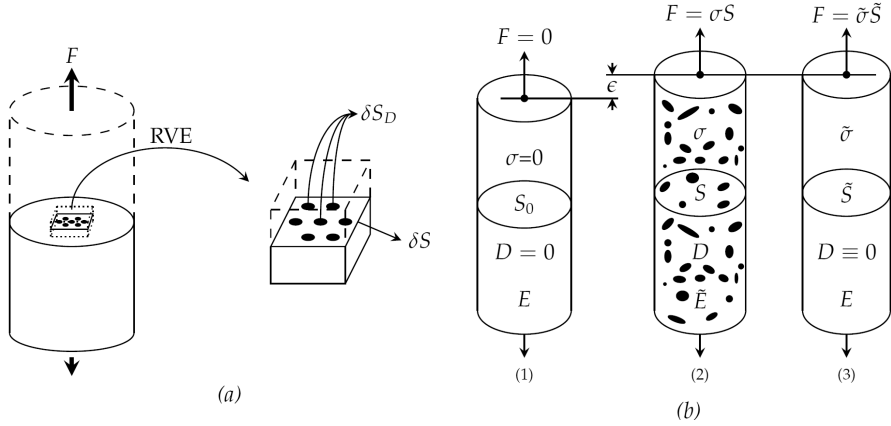$$\tilde{\sigma} = \frac{\sigma}{1 - D} \tag{5}$$

*Figure 10. (a) Scalar damage representation, (b) Deformation and damage in one-dimension;*
*1 - undamaged state; 2 - damaged state; 3 - fictitious undamaged state $\tilde{S}$ = (1 - D)S*

Beside the effective area reduction, damage quantification can also be based on the variation of the effective elastic modulus $E$ of the material. In order to do so, the concept of strain equivalence principle [Lemaitre, 1971] is introduced. The principle states that the strain of a damaged continuum $\varepsilon(\sigma,D)$ is equivalent to strain of the (fictitious) undamaged continuum $\varepsilon(\tilde{\sigma}, D \equiv 0)$ with the usual stress replaced by the effective stress (illustrated in Figure 10(b)). After a simple derivation using the strain equivalence principle, the damage variable can be described as a function of the effective elastic modulus written as follows,

$$D = 1 - \frac{\tilde{E}}{E} \tag{6}$$

where $\tilde{E}$ is the elastic modulus of the damaged material which varies linearly with the damage variable $D$. The damage definition given in Eq. (6) is the most common method to experimentally measure damage in a material. Figure 11 shows the elastic modulus reduction during cyclic loading as a result of damage growth.

The scalar damage definition (Eq. (4) and Eq. (6)), resulting in isotropic damage, is the simplest approach of CDM and is sufficient to describe material deterioration induced by microplasticity such as in HCF [Lemaitre, 1984; Lemaitre & Desmorat, 2005].

### 3.3   *Critical damage criterion*

From the definition of Eq. (4) and Eq. (6), the value of the damage variable $D$ is bound by 0

and 1 ($0 \leq D \leq 1$), where $D = 0$ for the undamaged RVE and $D = 1$ for the fully broken RVE. However, in many cases failure of the RVE occurs for $D < 1$ due to a process where sudden decohesion of atoms occurs in the remaining resisting area of the RVE. The value of $D$ at which this applies is called the critical damage $D_c$. Its value strongly depends on the material structure, the failure mechanism and the condition of loading. The value may vary between $D_c \approx 0$ for pure brittle fracture to $D_c \approx 1$ for pure ductile fracture. In most cases, $D_c$ ranges from 0.2 to 0.5 [Lemaitre, 1996]. Mesocrack initiation occurs when the damage reaches $D_c$ for isotropic damage.

# 4    Continuum damage models for fatigue life prediction

This chapter elaborates a number of existing fatigue damage models based on CDM. Although some models given in this section have been used to model fatigue crack growth, the summaries provided here remain solely focused on fatigue crack initiation. An evaluation of the models is provided in Section 6.

## 4.1    Chaboche model

This phenomenological model, proposed by [Chaboche, 1974], is based on a generalization of the model of [Marco & Starkey, 1954] and the damage curve approach by [Manson & Halford, 1981]. It is a simple engineering tool to predict the fatigue life of structures up to macrocrack initiation. Similar to the total life approach using the S-N curve, this model describes the damage evolution in each cycle as function of the maximum stress $\sigma_{max}$, the
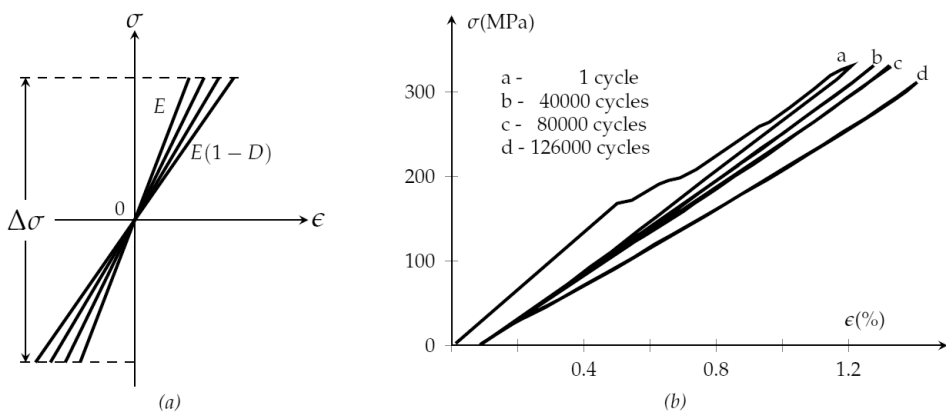


Figure 11. (a) Elastic moduli reduction due to damage in HCF (b) Stress-strain curve of graphite/epoxy composite at various stages fatigue life (R = 0.1) [Daniel & Charewicz, 1986]

mean stress $\sigma_m$ and the total damage variable $D$. However, the non-linearity of damage evolution is taken into account using CDM which provides an indirect measure of fatigue damage (degradation of modulus elasticity as a function of fraction of number of cycles). The damage evolution function is written as [Chaboche & Lesne, 1988; Chaboche, 1974]:

$$dD = \left[1-(1-D)^{\beta+1}\right]^{\alpha} \left[\frac{\sigma_{\max} - \sigma_m}{M(\sigma_m)(1-D)}\right]^{\beta} dN \tag{7}$$

with $M(\sigma_m) = M_0(1-b\,\sigma_m)$. The function $M(\sigma_m)$ is introduced to describe the linear relationship between the mean stress and the fatigue limit. The coefficient $\alpha$ is given as:

$$\alpha = 1 - a\left\langle \frac{\sigma_{\max} - \sigma_f(\sigma_m)}{\sigma_u - \sigma_{\max}} \right\rangle \quad \text{with} \quad \sigma_f(\sigma_m) = \sigma_m + \sigma_f^{\infty}(1-b\sigma_m) \tag{8}$$

The symbol $\langle\ \rangle$ defines as $\langle x \rangle = 0$ if $x < 0$ and $\langle x \rangle = $ x if x > 0. The parameters $\alpha$, $\beta$, $M_0$ and $b$ are material dependent. The parameter $\sigma_f^{\infty}$ is the fatigue limit for fully reversed loading conditions ($R = -1$), $\sigma_u$ is the ultimate stress, $\sigma_f(\sigma_m)$ is the fatigue limit for a non-zero mean-stress.

The damage $D$ and the number of cycles to macrocrack initiation $N_F$ are determined by integrating Eq. (7) for constant $\sigma_{\max}$ and $\sigma_m$ between $D = 0$ and $D = 1$. Combined with Eq. (8), this gives:

$$D = 1 - \left[1 - \left(\frac{N}{N_F}\right)^{\frac{1}{1-\alpha}}\right]^{\frac{1}{\beta+1}}, \qquad N_F = \frac{1}{(\beta+1)(1-\alpha)}\left[\frac{\sigma_{\max} - \sigma_m}{M(\sigma_m)}\right]^{-\beta} \tag{9}$$

The material parameters and coefficients are easily determined from conventional test data, including the S-N curve for crack initiation as described in [Chaboche & Lesne, 1988].

## 4.2    *Peerlings model*

The fatigue damage model by [Peerlings, 1999] describes damage due to HCF through deterioration of the stiffness moduli of the material. The model assumes that the damage development does not introduce anisotropic material behaviour. Thus, a single scalar damage variable $D$ is sufficient to describe the local damage state of the material. The effect of the damage on stresses is given as [Lemaitre & Chaboche, 1990],

$$\sigma_{ij} = (1-D)C_{ijkl}\,\varepsilon_{kl} \ , \qquad C_{ijkl} = \frac{E\nu}{(1+\nu)(1-2\nu)}\delta_{ij}\delta_{kl} + \frac{E}{2(1+\nu)}(\delta_{ik}\delta_{jl} + \delta_{il}\delta_{jk}) \tag{10}$$

with $\sigma_{ij}$ $(i, j = 1, 2, 3)$ is stress component, $\varepsilon_{kl}$ $(k, l = 1, 2, 3)$ is the strain and $\delta$ is the Kronecker delta. The effective stiffness moduli $(1 - D)\,C_{ijkl}$ decrease as damage accumulates, which results in complete loss of the mechanical integrity when the damage reaches the critical value which is regarded as crack initiation.

As the material is continuously loaded, the damage variable which affects the strain-stress relationship (Eq. (10)) will evolve. The damage evolution is assumed to start only when a specified limit is exceeded. The model defines this limit, which is also referred to as damage loading surface (Figure 12), in terms of strain. The damage loading surface is given as follows,

$$f(\varepsilon, \kappa) = \tilde{\varepsilon}(\varepsilon) - \kappa \tag{11}$$

where $\tilde{\varepsilon}$ is a scalar representing the equivalent measure of the strain state or equivalent strain and $\kappa$ is a threshold parameter. The damage loading surface $f = 0$ is corresponding to the fatigue limit of the material. For $f < 0$, the strain state is within the damage loading surface, thus, there will be no damage. If the equivalent strain is equal to or greater than the threshold $\kappa$, the damage loading function $f \geq 0$ is reached and the damage increases. The von Mises strain is selected to define the equivalent strain, which is given as,

$$\tilde{\varepsilon} = \frac{1}{1+\nu}\sqrt{-3J_2} \ , \text{ where } J_2 = \tfrac{1}{6}I_1^2 - \tfrac{1}{2}\varepsilon_{ij}\varepsilon_{ij} \text{ and } I_1 = \varepsilon_{kk} \tag{12}$$

Besides the condition $f \geq 0$, the model assumes that the damage variable can only increase for continued loading $\dot{f} \geq 0$ and it remains constant during unloading. The damage growth
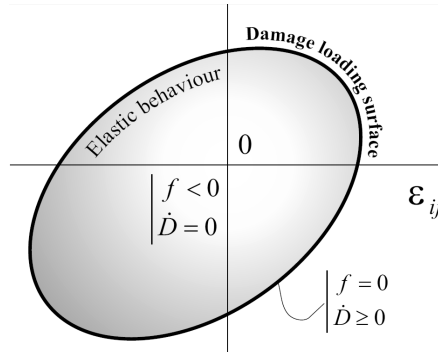


*Figure 12. Damage loading surface defined in strain space*

function during loading is given as,

$$\dot{D} = \begin{cases} g(D,\tilde{\varepsilon})\dot{\tilde{\varepsilon}} & \text{if } f \geq 0 \text{ and } \dot{f} \geq 0 \text{ and } D < 1 \\ 0 & \text{otherwise} \end{cases} \quad \text{with } g(D,\tilde{\varepsilon}) = Ce^{\alpha D}\tilde{e}^{\beta} \tag{13}$$

where $\dot{\tilde{\varepsilon}}$ is the strain rate and $C$, $\alpha$ and $\beta$ are material parameters.

The constitutive model given above together with the equilibrium equations and boundary conditions are solved using the finite element (FE) method. The loading history is divided into a finite number of time increments and the damage growth is integrated within these increments. The details of obtaining the linear system of equations along with the method to integrate the damage in a large number of cycles within each increment is given in [Peerlings et al., 2000].

One advantage of this model is that application of complex loading is a straightforward procedure. In uniaxial, fully reversed constant amplitude strain $\varepsilon_a$, the damage growth and the fatigue life (Eq. (13)) can be solved in closed form. It is assumed that the equivalent strain equals the strain amplitude at both extremes (i.e. in tension and compression) and that there is no fatigue limit ($\kappa = 0$). Integration of Eq.(13) over $N$ cycles, after substituting $g(D,\tilde{\varepsilon})$ and setting $D = 1$, gives the following number of cycles to failure.

$$N_f = \frac{\beta+1}{2\alpha C}(1 - e^{-\alpha})e_a^{-(\beta+1)} \tag{14}$$

Material parameters $C$, $\alpha$ and $\beta$ are determined by modification of Eq. (14) to the high cycle part of the strain-based approach of [Basquin, 1910] as given in [Peerlings et al., 2000].

### 4.3   *Chow model*

The Chaboche model described previously faces two fundamental unresolved problems. The first problem is the definition of the multiaxial stress parameters associated with the maximum stress and mean stress. The second problem is the inadequate formulation in the case of complex loading as described in Section 2.2.3. In order to tackle these problems, Chow developed a constitutive damage model of fatigue failure [Chow &Wei, 1991, 1999]. This fatigue damage model offers an interesting combination between a phenomenological approach and micromechanical modelling of material degradation.

The model introduces a damage tensor that consists of two scalar damage variables. These scalars are introduced to take into account the Poisson's ratio change (represented by the damage variable $\mu_f$) during tension loading (experimentally observed in [Chow &Wang,

1987]) in addition to the change in the elastic modulus (represented by the damage variable $D_f$). The damage evolution function for the two damage variables are postulated within the framework of irreversible thermodynamics described as follows,

$$dD_f = -dw_f \frac{Y_{Df}}{2Y_{fd}^{1/2}} \ , \quad d\mu_f = -dw_f \frac{\gamma Y_{\mu f}}{2Y_{fd}^{1/2}} \ , \quad dw_f = \frac{Y_{Df}dY_{Df} + \gamma Y_{\mu f}dY_{\mu f}}{2Y_{fd}^{1/2}K(w_f)} \tag{15}$$

with $D(w_f) = K_0(1 - \dfrac{w_f}{w_c})$ and $Y_{fd}$ is given as,

$$Y_{fd} = \tfrac{1}{2}(Y_{Df}^2 + \gamma Y_{\mu f}^2) \ \text{ with } Y_{Df} = -\frac{1}{1-D_f}\sigma^T : \mathbf{C}^{-1} : \sigma \ \text{ and } \ Y_{\mu f} = -\frac{1}{1-D_f}\sigma^T : \mathbf{A} : \sigma \tag{16}$$

where $\sigma$, $\sigma^T$ are stress and stress transpose; $\gamma$ and $K_0$ are material dependent parameters; $\mathbf{C}(D_f, \mu_f)$ and $\mathbf{A}(D_f, \mu_f)$ are the damage effect tensors; $w_f$ and $w_c$ are the overall fatigue damage and the critical value of the overall fatigue damage, respectively.

The contribution of a tensile stress to the fatigue damage accumulation is different from that of a compressive stress due to closure of some microcracks. To take into account this phenomenon, the stress $\sigma$ in $Y_{Df}$ and $Y_{\mu f}$ is replaced with the active stress $\sigma_{act}$. In the uniaxial case, for reversed loading (stress ratio less than zero) condition $\sigma_{act} = \sigma - \alpha\sigma_{min}$ and in full compression loading $\sigma_{act} = \alpha(\sigma - \sigma_{min})$, where $\alpha$ is the damage efficiency factor (a material parameter which varies from 0 to 1).

In the case of HCF, where overall plasticity is negligible, fatigue damage accumulation per cycle is calculated using Eq. (15) and written as,

$$\frac{\Delta D_f}{\Delta N} = \int_{\sigma_c}^{\sigma_{max}} dD_f \ , \quad \frac{\Delta\mu_f}{\Delta N} = \int_{\sigma_c}^{\sigma_{max}} d\mu_f \ , \quad \frac{\Delta w_f}{\Delta N} = \int_{\sigma_c}^{\sigma_{max}} dw_f \tag{17}$$

where $\sigma_c$ is the stress tensor determined by the damage surface $F_{fd}(\sigma_c) = Y_{fd}^{1/2} - B_{0f} = 0$ with $B_{0f}$ is a material dependent parameter related to the fatigue endurance limit.

Implementation of the model using FE can be performed through a user material subroutine (usually available in commercial FE codes) where for a given loading history, the overall fatigue damage $w_f$ is calculated by solving the constitutive model. If $w_f$ reaches its critical value $w_c$, a material element is said to have broken and a crack is initiated. As in Peerling's model, this model also provides a straightforward procedure for a complex loading condition with the advantage of different damage accumulation between tension and compression loading.

44

The material parameters γ, $K_0$, α, $B_{0f}$ and $w_c$ needed for this model are determined from monotonic tensile and stress-controlled uniaxial fatigue tests. The details of the procedures to obtain these parameters are given in [Chow &Wei, 1999].

### 4.4 Lemaitre model

Contrary to the previous models, the two scale fatigue model by [Lemaitre *et al.*, 1999] offers the possibility to account for micro-plasticity and micro-damage which characterize HCF. In HCF, damage and plasticity occur at the microscale and have no influence on the elastic macroscopic behaviour except in the failure stage [Lemaitre *et al.*, 1999]. This model describes the fatigue process prior to macrocrack initiation.

The model considers a representative volume element in a body and it postulates that inside the RVE, a micoscale volume $M$ is included (i.e. inclusion). The model is schematically described in Figure 13, where the superscripts μ, *e* and *p* refer to microscopic
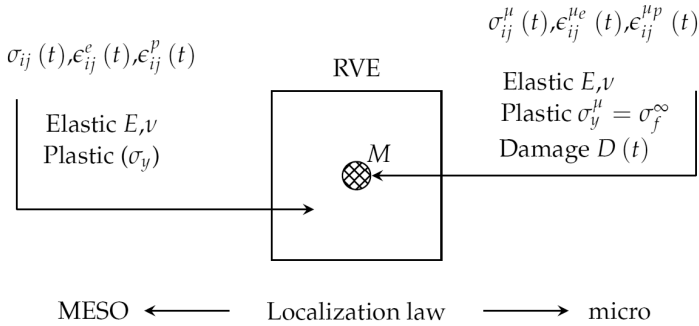


*Figure 13: Micro-element embedded in elastic RVE [Lemaitre & Desmorat, 2005]*

variables, elastic properties and plastic properties, respectively. The matrix that surrounds the inclusion has elastic properties $E$, ν of the RVE. The inclusion $M$ itself has the same elastic properties as the matrix but it undergoes plastic deformation and is subjected to damage. The yield stress of the inclusion is taken equal to the fatigue limit of the material $\sigma_f^\infty$. Thus, neither plasticity nor damage occur below this value. When the damage variable reaches a critical value, the inclusion is broken which corresponds to fatigue macrocrack initiation.

At the mesoscale, the stress is denoted as σ and the total, elastic and plastic strains are denoted as ε, $\varepsilon^e$ and $\varepsilon^p$, respectively. Their values are known from a FE computation. As for HCF, the plastic strain $\varepsilon^p$ is considered zero.

In order to describe the damage development at microscale, the stress and strain state of volume $M$ have to be known. These entities are evaluated using the Eshelby-Kröner localization law of micromechanics [Eshelby, 1957; Kroner, 1961] which relates the strain at microscale to the mesoscopic strain. For a spherical inclusion, the localization law reads,

$$\varepsilon_{ij}^{\mu} = \varepsilon_{ij} + \beta(\varepsilon_{ij}^{\mu p} - \varepsilon_{ij}^{p}) \quad \text{with} \quad \beta = \frac{2}{15}\frac{4-5\nu}{1-\nu} \tag{18}$$

The strain in the inclusion is divided into an elastic part and a plastic part $\varepsilon_{ij}^{\mu} = \varepsilon_{ij}^{\mu e} + \varepsilon_{ij}^{\mu p}$ where the elastic part is written as

$$\varepsilon_{ij}^{\mu e} = \frac{1+\nu}{E}\frac{\sigma_{ij}^{\mu}}{1-D} - \frac{\nu}{E}\frac{\sigma_{kk}^{\mu}}{1-D}\delta_{ij} \tag{19}$$

The damage loading surface ($f^{\mu} = 0$) of the inclusion, considering linear kinematic hardening, is given as

$$f^{\mu} = (\tilde{\sigma}^{\mu} - X^{\mu})_{eq} - \sigma_{f}^{\infty} \tag{20}$$

with $(.)_{eq}$ is the von Mises equivalent, $\tilde{\sigma}^{\mu} = \dfrac{\sigma^{\mu}}{1-D}$ is the effective stress and $X^{\mu}$ is the microscale back stress.

The set of constitutive equations for plastic strain, linear kinematic hardening and damage evolution law is:

$$\dot{\varepsilon}_{ij}^{\mu p} = \frac{3}{2}\frac{\tilde{\sigma}_{ij}^{\mu D} - X_{ij}^{\mu}}{(\tilde{\sigma}_{\mu} - X^{\mu})_{eq}}\dot{p}^{\mu}, \qquad \dot{X}_{ij}^{\mu} = \frac{2}{3}C_{y}(1-D)\dot{\varepsilon}_{ij}^{\mu p} \tag{21}$$

$$\dot{D} = \left(\frac{Y^{\mu}}{S}\right)^{s}\dot{p}^{\mu} \quad \text{if} \quad p^{\mu} > p_{D}^{\mu}, \quad D = D_{c} \tag{22}$$

If $D$ reaches the critical value $D_{c}$, the crack initiates. The superscript $D$ denotes the deviatoric properties $(.)_{ij}^{D} = (.)_{ij} - (1/3)\delta_{ij}(.)_{kk}$, $p^{\mu}$ is the accumulated plastic strain and the plastic modulus $C_{y}$, the damage strength $S$ and the damage exponent $s$ are material dependent parameters. The damage energy release rate $Y^{\mu}$ is given as,

$$Y^{\mu} = \frac{1+\nu}{2E}\left[\frac{\langle\sigma^{\mu}\rangle^{+}\langle\sigma^{\mu}\rangle^{+}}{(1-D)^{2}} + h\frac{\langle\sigma^{\mu}\rangle^{-}\langle\sigma^{\mu}\rangle^{-}}{(1-hD)^{2}}\right] - \frac{\nu}{2E}\left[\frac{\langle\sigma_{kk}^{\mu}\rangle^{2}}{(1-D)^{2}} + h\frac{\langle-\sigma_{kk}^{\mu}\rangle^{2}}{(1-hD)^{2}}\right] \tag{23}$$

where the $\left\langle \sigma^\mu \right\rangle^+$ and $\left\langle \sigma^\mu \right\rangle^-$ denote the positive and negative parts of the principle stress tensor, respectively. A smaller damage growth during compression due to micro-defects closure is accounted for by parameter $h$. An often applied value for metals is $h = 0.2$ [Lemaitre & Desmorat, 2005]. The plastic damage threshold $p_D^\mu$ is calculated as,

$$p_D^\mu = \varepsilon_{pD} \left( \frac{\sigma_u - \sigma_f^\infty}{\frac{1}{2}(\Delta\sigma^\mu)_{eq} - \sigma_f^\infty} \right)^m \tag{24}$$

with $\varepsilon_{pD}$ is the plastic threshold at monotonic uniaxial tension and $m$ is a material dependent parameter. The material parameters $S$, $s$, $\varepsilon_{pD}$, $m$ and $D_c$) can be identified by the 'fast identification method' given in [Lemaitre & Desmorat, 2005]. The method requires results from tensile tests as well as low and high cycles fatigue tests.

The model accounts not only for complex loading and micro-defects closure, but also for microplasticity, which is an important physical feature of HCF. Moreover, HCF damage is influenced by the initial state of the materials, i.e. the initial plastic strain and the initial damage which are induced by the thermo-mechanical history of casting, metal forming, welding, and also damages by accident. These initial conditions can be introduced into the model as initial values $\varepsilon^p = \varepsilon_0^p$ and $D(t = 0) = D_0$.

### 4.5    *Application example of Lemaitre model*

In [Lemaitre & Desmorat, 2005], an application example of their two scale fatigue damage model is described. The model is used to predict the crack initiation period of a tubular component. The middle part of the tube is thinned to facilitate crack initiation (Figure 14(a)). The total length of the tube is $L = 250$ mm with inner radius of $r = 27.5$ mm. The thickness of the thinned part varies from 1.2 to 0.6 mm. The tube was loaded in tension-torsion with proportional and non-proportional ($90^0$ out of phase) loading conditions. The maximum applied force and torque are $F_{max} = 14000$ N and $C_{max} = 420$ Nm, respectively. The mesoscale variables are obtained through an elastic FE analysis of the tube. The history of (elastic/plastic) strains and stresses at every instant (time $t$) at the thinned part are known from this reference computation. As the microscale variables at $t_n$ and the mesoscale variables at $t_n$ and $t_n + 1$ are known, the microscale variables at $t_n + 1$ can be determined as follows [Lemaitre & Desmorat, 2005],

- A **local elastic prediction** assumes elastic behaviour ($\varepsilon^{\mu p} = \varepsilon_n^{\mu p}$, $X^\mu = X_n^\mu$ and $D = D_n$), which gives the following variables,

$$\varepsilon^\mu = \varepsilon + \beta(\varepsilon_n^{\mu p} - \varepsilon_{n+1}^p), \quad \tilde{\sigma}^\mu = \sigma - 2G(1-\beta)(\varepsilon_n^{\mu p} - \varepsilon_{n+1}^p) \tag{25}$$

- A **local plastic predictor** is used. If the variables obtained from the elastic predictor satisfy $f^\mu \leq 0$, the $\tilde{\sigma}_{n+1}^\mu = \tilde{\sigma}^\mu$, $\varepsilon_{n+1}^\mu = \varepsilon^\mu$ and $\varepsilon_{n+1}^{\mu e} = \varepsilon^{\mu e}$ are set. Otherwise, the following non-linear equation has to be solved using the Newton iterative scheme:

$$\begin{aligned}
R_s &= s_{n+1}^\mu + \tfrac{2}{3}\mathbf{G}m_{n+1}^\mu \Delta p^\mu - \mathbf{E} : \varepsilon_{n+1} + 2G\beta\varepsilon_{n+1}^p + 2G(1-\beta)\varepsilon_n^{\mu p} + X_n^\mu = 0 \\
R_p &= (s_{n+1}^\mu)_{eq} - \sigma_f^\infty = 0
\end{aligned} \tag{26}$$

where $s^\mu = \tilde{\sigma}^\mu - X^\mu$, $\mathbf{G} = 3G(1-\beta) + C_y(1-D_n)$, $G = \dfrac{E}{2(1+\nu)}$, $m^\mu = \tfrac{2}{3}(s^{\mu D}/s_{eq}^\mu)$, $\Delta p^\mu = p_{n+1}^\mu - p_n^\mu$ $\nu$ and $\mathbf{E}$ is the elastic tensor. After convergence, $\Delta p$ and $s_{n+1}^\mu$ are obtained and the rest of the variables at $t_{n+1}$ including $D_{n+1}$ can be determined. The process is repeated until $D_c$ is reached.

The material parameters (ductile steel) used in the simulation are: $E = 200\,\text{GPa}$, $\nu = 0.3$, $\sigma_y = 380\,\text{MPa}$, $\sigma_u = 474\,\text{MPa}$, $C_y = 50\,\text{GPa}$, $\sigma_f^\infty = 180\,\text{MPa}$, $\varepsilon_{pD} = 0.05$, $m = 3$, $S = 2.6\,\text{MPa}$, $s = 2$, $h = 0.2$ and $D_c = 0.3$. Figure 14(b) gives the comparison between the number of cycles to crack initiation according to tests $N^{\exp}$ and the number of cycles to crack initiation
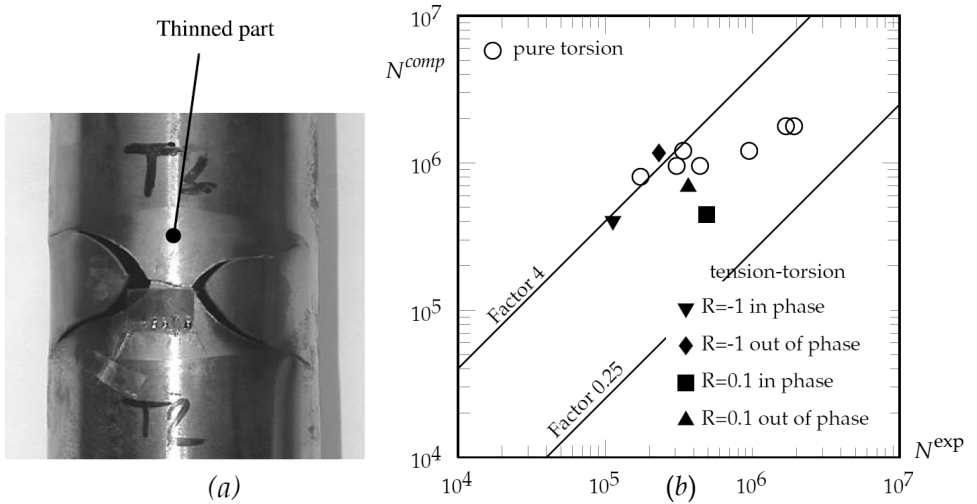


Figure 14. (a) A thinned tube (b) Two-scale fatigue model predictions [Lemaitre & Desmorat, 2005]

according to the computation $N^{\text{comp}}$ of the thinned tube with pure torsion and tension-torsion cyclic loads. Figure 14 indicates that the number of cycles at failure is predicted with reasonable accuracy, especially when bearing in mind that the fatigue life is subjected to significant scatter.

## 5    Cohesive zone model

### 5.1    Introduction

In this section as opposed to the previous section, a discontinuous approach to fatigue fracture is presented. Where the CDM is dedicated to crack initiation, the cohesive zone model (CZM) given in this section is aimed at describing crack propagation. The concept of CZM was first introduced by Dugdale [Dugdale, 1960] and Barenblatt [Barenblatt, 1962]. A cohesive zone is placed in front of the physical crack tip at a predefined crack path. Separation between two adjacent virtual surfaces is resisted by the presence of the cohesive traction. The cohesive traction represents the inter-atomic forces and acts as the resistance to crack propagation. During loading, the atomic structure changes and this can be reflected by variations in the cohesive traction. A cohesive law defines the traction as a function of the separation of the boundaries of the cohesive zone. It describes the constitutive behaviour of the CZM.

As discussed in Section 2.1.3, the mechanism of fatigue crack growth consists of plastic blunting and subsequent sharpening of the crack tip. The crack tip opening displacement during blunting directly influences the crack extension during sharpening where a larger displacement results in a longer crack extension. Therefore, it is convenient to use the cohesive zone model to describe fatigue crack growth as it directly deals with crack tip opening (separation).

There is a great variety in Traction-Separation Laws (TSLs) (summarized in [Chandra *et al.*, 2002]) but they all exhibit the same global behaviour. Upon the application of external loads to a cracked body (Figure 15 shows TSL in normal direction), the cohesive surfaces separate gradually leading to an increase in traction $T_n$ until a maximum value $\sigma_{\text{max},0}$ is reached. This maximum is called the cohesive strength. The traction decreases to approximately zero as the separation $\Delta_n$ reaches a critical value $\delta_{\text{sep}}$ .
In a cohesive zone, the progressive deterioration of the material strength in front of the crack tip is represented by the reduction of the cohesive traction.
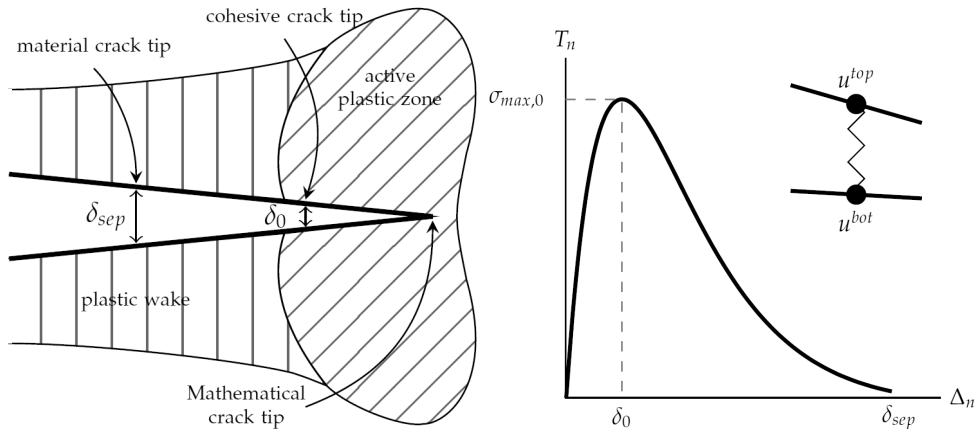
Figure 15: Cohesive process zone [Shet & Chandra, 2002]

## 5.2 Cohesive zone formulation

Using the principle of virtual work, the mechanical equilibrium considering the effect of the cohesive tractions is written as

$$\int_V \sigma : \delta\varepsilon dV - \int_{S_{\text{int}}} T_{CZ} \cdot \delta\Delta dS = \int_{S_{\text{ext}}} T_e \cdot \delta u dS \tag{27}$$

where $V$ is the specimen volume, $S_{\text{int}}$ is the internal cohesive surface and $S_{\text{ext}}$ is the external surface (Figure 16), $\sigma$ is the Cauchy stress tensor, $\varepsilon$ is the strain tensor, $u$ is the displacement vector, $T_{CZ}$ denotes the cohesive traction vector, $T_e$ is the external traction vector and $\Delta$ is a vector representing the separation displacement across the two adjacent cohesive surfaces. The cohesive tractions consist of normal and tangential components: $T_{CZ} = T_n n + T_t t$ . Symbols $n$ and $t$ denote the unit vectors normal and tangent to the
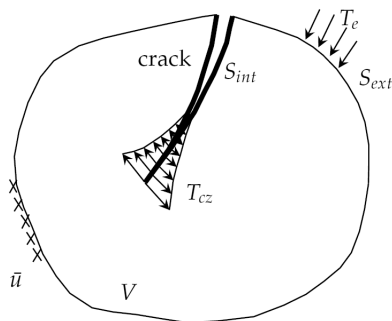


Figure 16: Schematic representation of mechanical equilibrium using CZM

50

cohesive surface, respectively. The separation displacement vector, $\Delta = \Delta_n n + \Delta_t t$ , is calculated from the displacements ( $u^{top}$ and $u^{bot}$ in Figure 15) of the opposing cohesive surfaces, where $\Delta_n$ and $\Delta_t$ are the normal and tangential separation displacements, respectively.

One of the most common TSL is an exponential traction law [Needleman, 1990] given as follows,

$$
\begin{aligned}
T_n &= \sigma_{max,0} e \exp\left(-\frac{\Delta_n}{\delta_0}\right)\left\{\frac{\Delta_n}{\delta_0}\exp\left(-\frac{\Delta_t^2}{\delta_0^2}\right)+(1-q)\frac{\Delta_n}{\delta_0}\left[1-\exp\left(-\frac{\Delta_t^2}{\delta_0^2}\right)\right]\right\} \\
T_t &= 2\sigma_{max,0} e q \frac{\Delta_t}{\delta_0}\left(1+\frac{\Delta_n}{\delta_0}\right)\exp\left(-\frac{\Delta_n}{\delta_0}\right)\exp\left(-\frac{\Delta_t^2}{\delta_0^2}\right)
\end{aligned}
$$

(28)

where $\delta_0$ is called the characteristic length which describes the separation required to reach the cohesive strength in normal loading (Figure 15), $e = \exp(1)$, $q$ is the coupling representation between normal and shear tractions i.e. the ratio between the area under the functions of pure tangential and pure normal traction.

## 5.3 *Damage mechanism*

Simulation of crack propagation under cyclic loading is conducted by introducing a damage mechanism into the cohesive zone that describes the material degradation due to accumulated irreversible deformation. The amount of material degradation can be quantitatively represented by a damage variable ($0 \leq D \leq 1$). A value in between 0 and 1 results in a reduced cohesive stiffness.

The cohesive traction function depends on the current state of damage as well as the current separations which leads to an irreversible and history dependent traction-separation equation. Using the *effective stress* concept [Lemaitre, 1996], the damage variable is incorporated into the TSL of Eq. (28) by replacing the initial cohesive strength of the undeteriorated material $\sigma_{max,0}$ with the current cohesive strength of the deteriorated material given as [Roe & Siegmund, 2003],

$$\sigma_{max} = \sigma_{max,0}(1-D) \, ,$$

(29)

where $D = \int_t \dot{D}dt$ . The damage evolution function $\dot{D}$ is given as,

$$\dot{D} = \frac{\left|\dot{\bar{\Delta}}\right|}{\delta_{sep}}\left[\frac{\bar{T}}{\sigma_{max}}-C_f\right]H(\bar{\Delta}-\delta_0) \text{ and } \dot{D} \geq 0$$

(30)

where $H$ is the Heaviside function and $\dot{\bar{\Delta}}$ is the rate of the displacement resultant. The parameters $\dot{\Delta}$, $\bar{T}$ and $C_f$ are given as,

$$\bar{\Delta} = \sqrt{\Delta_n^2 + \Delta_t^2} \ , \quad \bar{T} = \sqrt{T_n^2 + \frac{T_t^2}{2eq^2}} \ , \quad C_f = \frac{\sigma_f^c}{\sigma_{\max,0}} \ , \quad 0 < C_f < 1 \tag{31}$$

where $\sigma_f^c$ the cohesive zone endurance limit which is related to the fatigue threshold. In order to properly describe fatigue crack propagation under cyclic loading, the paths of unloading and reloading need also to be considered for the irreversible CZM (illustrated in Figure 17). In [Wang & Siegmund, 2006], the unloading-reloading path in normal and tangential loading direction are given as,

$$T_n = T_{n,\max} + \frac{T_{n,\max}}{\Delta_{n,\max}}(\Delta_n - \Delta_{n,\max}) \ , \quad T_t = T_{t,\max} + \sqrt{2e}\frac{\sigma_{\max}}{\delta_0}(\Delta_t - \Delta_{t,\max}) \tag{32}$$

where $\Delta_{n,\max}$ is the maximum value of normal separation before unloading and $T_{n,\max}$ is the corresponding normal traction (Eq. (28)) with $\sigma_{\max,0}$ replaced by $\sigma_{\max}$. A similar definition is also applied to the tangential direction.
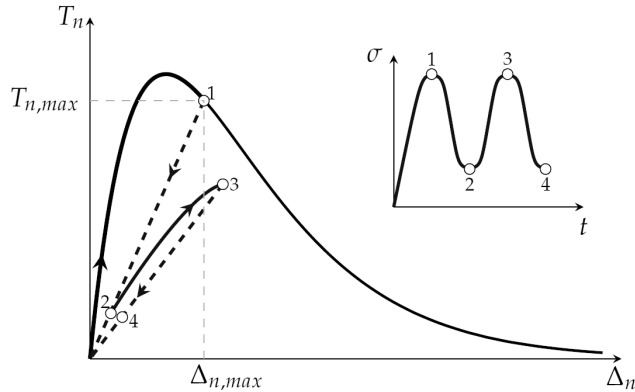


Figure 17: Schematic representation of unloading and reloading behaviour during cyclic loading; reduction of the cohesive strength due to accumulation of damage

## 5.4   Cohesive Parameters

The cohesive parameters include the cohesive strength $\sigma_{\max,0}$, the characteristic length $\delta_0$, the cohesive energy $\phi$ and the cohesive zone endurance limit $\sigma_f^c$. The endurance limit which is represented by the ratio $C_f$ is set to be 0.25 [Roe & Siegmund, 2003]. The cohesive strength is related to the yield stress of the bulk material ($\approx 2\sigma_y$ to $3\sigma_y$) [Chen & Kolednik,

2005]. The cohesive energy is equal to the area under the TSL (Figure 15) and for an exponential TSL as given previously, the cohesive energy is $\phi = \sigma_{max,0}\, e\, \delta_0$ . This energy is equal to the fracture energy $G_c$ of the material [Chen & Kolednik, 2005].

*5.5    FE implementation*

Implementation of the model in FE consists of describing the cohesive element constitutive behavior according to the TSL as well as the damage definition. Zero thickness cohesive elements are placed in front of a predefined crack path and their upper and lower nodes are connected to the bulk elements. In the initial state, the cohesive element and the facing edges of the neighbouring bulk elements occupy the same spatial position; at deformed state, normal and tangential tractions are induced between the neighbouring bulk elements. The cohesive element stiffness matrix $\mathbf{K}_{coh}^{el}$ and the element force vector $\mathbf{f}_{coh}^{el}$ are given as,

$$\mathbf{K}_{coh}^{el} = \int_{-1}^{1} \mathbf{B}^T \Theta \mathbf{D} \Theta^T \mathbf{B} \det \mathbf{J} d\xi \,, \quad \mathbf{f}_{coh}^{el} = \int_{-1}^{1} \mathbf{B}^T \Theta \mathbf{T} \det \mathbf{J} d\xi \,, \tag{33}$$

where $\mathbf{B}$ is the shape function matrix, $\mathbf{J}$ is the Jacobian matrix, $\Theta$ is the transformation matrix, $x$ is element natural coordinate and the stiffness matrix $\mathbf{D}$ and $\mathbf{T}$ are defined as

$$\mathbf{D} = \begin{bmatrix} \dfrac{\partial T_t}{\partial \Delta_t} & \dfrac{\partial T_t}{\partial \Delta_n} \\ \dfrac{\partial T_n}{\partial \Delta_t} & \dfrac{\partial T_n}{\partial \Delta_n} \end{bmatrix} \,, \quad \mathbf{T} = \begin{bmatrix} T_t \\ T_n \end{bmatrix} \tag{34}$$

If the critical damage is reached, due to separation in cohesive elements during unloading and reloading, the cohesive element is said to be broken and the crack tip is extended.

*5.6    Application example of the fatigue crack growth model based on CZM*

In [Ural et al., 2009], an application of CZM to predict the fatigue crack growth rate including crack retardation due to an overload is given. A compact tension (CT) specimen made of aluminium alloy A356-T6 is loaded in tension with $P_{max}$ = 4144.4 N and $P_{max}$ = 3230 N with stress ratio R = 0.1 and R = 0.5, respectively. At the predefined crack path, 60 cohesive elements are placed inside 13080 bulk elements under plane strain assumption. A slightly different TSL, i.e. a triangle-based TSL, is used as well as a slightly modified damage function of Eq. (30). Cycle by cycle simulation of high cycle fatigue is prohibitively expensive. An extrapolation scheme was proposed to predict the crack growth life of the

specimens where a crack extension is estimated in a large number of cycles by a scaling function. Figure 18 shows comparison between experimental results and the prediction results of the model. The figure indicates that there is a moderate to reasonable agreement between the prediction and the test. More research is required in order to determine the cause of the scatter in the prediction results.
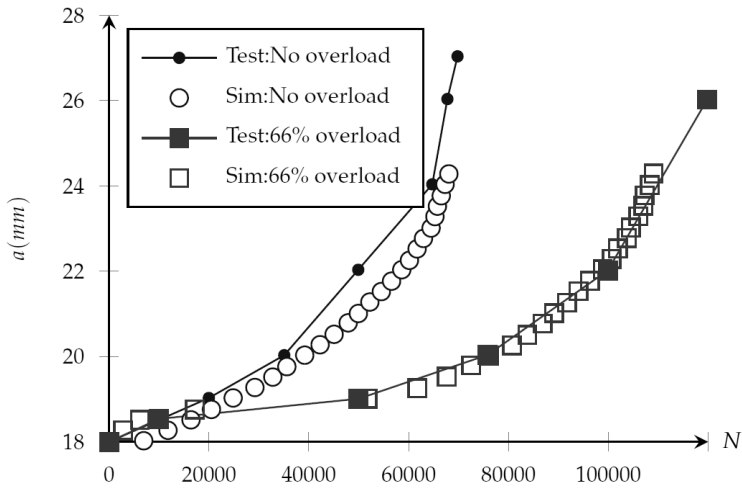


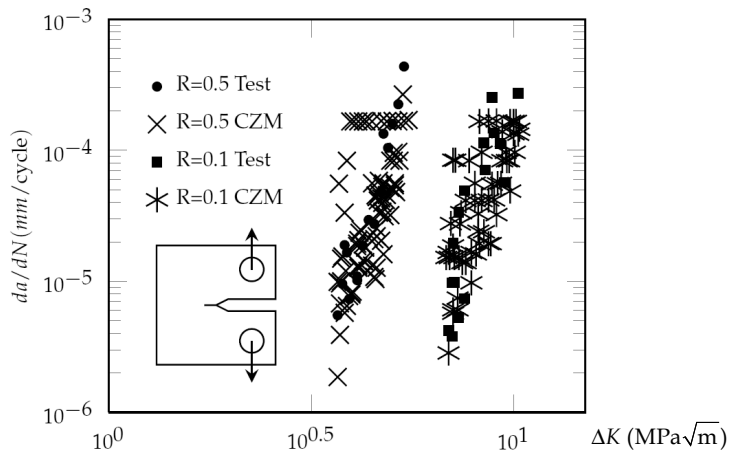*Figure 18a. Prediction results on crack retardation: the overload was applied at N = 4000 [Ural et al., 2009]*



*Figure 18b. Results of a CZM prediction on crack growth rate of aluminium alloy A356-T6 specimen [Ural et al., 2009]*

54

## 6    Evaluation and conclusion

The total fatigue life comprises of the crack initiation and the crack propagation periods. Crack initiation in metallic materials is caused by cyclic slip and is greatly influenced by the surface condition such as the surface roughness or the presence of a (sharp) notch. On the other hand, crack propagation involves the alternate blunting and sharpening of the crack tip and depends strongly on the material properties and the defect size. The theoretical background of any method to predict the crack initiation and/or crack propagation periods should be based on the corresponding mechanisms.

There are two engineering models widely used to predict the fatigue life of a structure or component. The model based on the S-N curves is strongly based on empirical data. The fatigue life prediction method based on linear elastic fracture mechanics (LEFM) has a physical background. However, it utilizes an empirical law to describe the relation between $\Delta K$ and $da/dN$. Application of these models is difficult or impossible in complex loading conditions such as multiaxial and non-proportional loading. Sequences in loads in case of variable amplitude loading influence the fatigue life, but this is poorly covered by both models.

Alternative models are summarized in this article based on continuum damage mechanics (CDM). Contrarily to the S-N curve model and the LEFM model, these models consider the fatigue process on a microlevel. The models can be implemented in numerical procedures, such as a FE model, to determine the fatigue life. The phenomenological CDM concept is shown to provide a good basis for crack initiation simulation. This paper summarizes four existing CDM based models dedicated to fatigue crack initiation.

Each of the CDM-based model describes the process during crack initiation using a damage accumulation mechanism. Due to loading, damage accumulates according to the damage mechanism up to a defined critical value which represents the crack initiation. Definition of damage mechanisms are different between models. A direct relation between the damage development and the loading configuration is found in Chaboche model. The damage mechanism in Peerling model relates the equivalent elastic strain due to the loading configuration to damage accumulation. In HCF, the elastic assumption is generally accepted at macroscale. On the other hand, Chow model offers a damage mechanism with two damage variables which is motivated by experimental observation. The damage mechanism relates the local stress and damage accumulation through thermodynamics potentials. In Lemaitre model, the damage mechanism is defined as a function of

accumulated plastic strain at microscale. It is a physically-motivated mechanism which describes the fatigue damage due to crystallographic slips (extrusion-intrusion).

The Chaboche model describes the deterioration processes before macrocrack initiation through a damage accumulation process which is obtained from indirect damage measurement. It is a simple engineering tool which includes the non-linear damage behavior in high cycle fatigue (HCF). Even though, this model offers no significant advantage compared to the S-N curve approach, it provides a first and important step towards more advanced models.

The fatigue damage model by Peerlings describes fatigue damage accumulation based on the equivalent elastic strain. The physical process involving microplasticity during crack initiation is not captured in this model. In addition, the difference in damage effects due to loads in tension and compression is also not present. However, application of complex loading is included.

The fatigue model by Chow takes into account the changes in elastic modulus and 311 Poisson's ratio due to fatigue damage. Similar to the Peerlings model, the ability of the model to describe fatigue under multiaxial loading, including shear is advantageous. Moreover, it also considers the difference between tension and compression in fatigue damage accumulation by introducing a damage efficiency factor.

Finally, the Lemaitre model includes an important physical feature in HCF, i.e. microplasticity at the crack tip that promotes microinitiation and micropropagation, as well as the other capabilities found in the previous models. Based on its good physical background together with several extra benefits as described previously, among all the models, the Lemaitre model is expected to give the most accurate prediction of fatigue crack initiation period.

A cohesive zone model gives an alternative approach to model crack propagation and/or fracture of materials. Application of the model in a FE analysis is relatively easy, which makes this approach attractive. The fatigue crack growth is simulated by incorporating a constitutive law that describes the damage development during unloading and reloading at the crack tip. The damage mechanism can be regarded as a representation of plastic-induced deterioration at the crack tip during cyclic loading. With a good damage mechanism definition, the effect of overloads on the crack growth behaviour can be naturally captured, which is beneficial compared to models based on LEFM where curve fitted parameters are required to capture the effect of overloads.

# References

Barenblatt, G.I. 1962. The Mathematical Theory of Equilibrium Cracks in Brittle Fracture. *Advances in Applied Mechanics*, 7, 55–129.

Basquin, O. H. 1910. The Exponential Law of Endurance Tests. Page 625 of: *American Society for testing of Materials*, vol. 10. West Conshochocken: ASTM.

Budiansky, B., & O'connell, R. J. 1976. Elastic moduli of a cracked solid. *International Journal of Solids and Structures*, 12, 81–97.

Cauvin, A., & Testa, R. B. 1999. Damage mechanics: basic variables in continuum theories. *International Journal of Solids and Structures*, 36, 636–650. 312

Chaboche, J. L., & Lesne, P. M. 1988. A Non-linear Continuous Fatigue Damage Model. *Fatigue & Fracture of Engineering Materials & Structures*, 11(1), 1–17.

Chaboche, J.L. 1974. Une loi différentielle d'endommagement de fatigue avec cumulation non linéaire. Rev. Franqaise de Mécanique, 50–51.

Chandra, N., Li, H., Shet, C., & Ghonem, H. 2002. Some issues in the application of cohesive zone models for metalceramic interfaces. *International Journal of Solids and Structures*, 39, 2827–2855.

Chen, C.R., & Kolednik, O. 2005. Comparison of Cohesive Zone Parameters and Crack Tip Stress States Between Two Different Specimen Types. *International Journal of Fracture*, 132, 135152.

Chow, C. L., & Wang, J. 1987. An anisotropic theory of elasticity for continuum damage mechanics. *International Journal of Fracture*, 33, 3–16.

Chow, C. L., & Wei, Y. 1991. A model of continuum damage mechanics for fatigue failure. *International Journal of Fracture*, 50(4), 301–316.

Chow, C. L., & Wei, Y. 1999. Constitutive Modeling of Material Damage for Fatigue Failure Prediction. *International Journal of Damage Mechanics*, 8(4), 355–375.

Daniel, I. M., & Charewicz, A. 1986. Fatigue damage mechanisms and residual properties of graphite/epoxy laminates. *Engineering Fracture Mechanics*, 25, 793–808.

Dowling, N. E., & Begley, J. A. 1976. Fatigue crack growth during gross plasticity and the J-integral. In: *ASTM STP 590 Mechanics of Crack Growth*.

Dugdale, D. S. 1960. Yielding of steel sheets containing slits. *Journal of the Mechanics and Physics of Solids*, 8, 100–104.

Elber, W. 1971. The Significance of Fatigue Crack Closure. In: *ASTM STP 486 Damage tolerance in aircraft structures*. American Society for Testing and Materials.

Eshelby, J. D. 1957. The Determination of the Elastic Field of an Ellipsoidal Inclusion, and Related Problems. *Proceedings of the Royal Society of London. Series A. Mathematical and Physical Sciences,* 241(1226), 376–396.

Forman, R. G. 1972. Study of fatigue crack initiation from flaws using fracture mechanics theory. *Engineering Fracture Mechanics*, 4(2), 333–345. 313

Griffith, A. A. 1921. The phenomena of rupture and flow in solids. *Philosophical Transactions of the Royal Society of London*. Series A, 221, 163–198.

Gurson, A. L. 1977. Continuum Theory of Ductile Rupture by Void Nucleation and Growth: Part I—Yield Criteria and Flow Rules for Porous Ductile Media. *Journal of Engineering Materials and Technology*, 99(1), 2–15.

Hashin, Z. 1983. Analysis of composite materials – A Survey. *Journal for Applied Mechanics, ASME Transactions*, 50, 481–505.

Hill, R. 1963. Elastic properties of reinforced solids: Some theoretical principles. *Journal of the Mechanics and Physics of Solids*, 11, 357–372.

Huang, X. P., Zhang, J.B., Cui, W.C., & Leng, J.X. 2005. Fatigue crack growth with overload under spectrum loading. *Theoretical and Applied Fracture Mechanics*, 44, 105–115. International, ASTM. 2002. *ASTM Standard E1823. 1996(2002). Standard Terminology Relating to Fatigue and Fracture Testing*. Tech. rept. ASTM International.

Kachanov, L. M. 1958. Rupture time under creep conditions. *International Journal of Fracture*, 97, 11–18.

Krajcinovic, D. 1984. Continuous damage mechanics. *Applied Mechanics Reviews*, 1, 1–6.

Krajcinovic, D. 1996. *Damage Mechanics*. Elsevier, The Netherlands.

Kroner, E. 1961. On the plastic deformation of polycrystals. *Acta Metallurgica et Materialia*, 9, 155–161.

Lemaitre, J. 1971. Evaluation of dissipation and damage in metals submitted to dynamic loading. Pages 540–549 of: *Proceedings of International Conference on the Mechanical behavior of materials (ICM1)*.

Lemaitre, J. 1984. How to use damage mechanics. *Nuclear Engineering and Design*, 80(2), 233–245.

Lemaitre, J. 1985. A Continuous Damage Mechanics Model for Ductile Fracture. *Journal of Engineering Materials and Technology*, 107(1), 83–89.

Lemaitre, J. 1996. *A course on damage mechanics*. 2nd rev. and enl. edn. Berlin ; New York: Springer. 96015592 (Jean), Jean Lemaitre ; with a foreword by H. Lippmann. ill. ; 24 cm. Includes bibliographical references (p. [222]) and index. 314

Lemaitre, J, & Chaboche, J. 1978. Aspect ph´enom´enologie de la rupture par endommagement. *J. Mécanique Appl.,* 2, 317–365.

Lemaitre, J., & Chaboche, J. L. 1990. *Mechanics of solid materials*. Cambridge University Press. Jean Lemaitre and Jean-Louis Chaboche.

Lemaitre, J., & Chaboche, J.L. 1974. A nonlinear model of creep-fatigue damage cumulation and interaction. In: *IUTAM Symposium of Mechanics of visco-elastic media and bodies*.

Lemaitre, J., & Desmorat, R. 2005. *Engineering damage mechanics : ductile, creep, fatigue and brittle failures.* Berlin ; New York: Springer. 2004111141 GBA452009 012954152 970929129 (Jean), J. Lemaitre, R. Desmorat. ill. ; 25 cm. Includes bibliographical references (p. [373]) and index.

Lemaitre, J., & Doghri, I. 1994. Damage 90: a post processor for crack initiation. *Computer Methods in Applied Mechanics and Engineering*, 115(3-4), 197–232.

Lemaitre, J., Sermage, J. P., & Desmorat, R. 1999. A two scale damage concept applied to fatigue. *International Journal of Fracture*, 97(1), 67–81.

Lubarda, V., & Krajcinovic, D. 1993. Damage Tensors and the Crack Density Distribution. *International Journal of Solids and Structures*, 30, 28592877.

Manson, S. S., & Halford, G. R. 1981. Practical implementation of the double linear damage rule and damage curve approach for treating cumulative fatigue damage. *International Journal of Fracture*, 17, 169–192.

Marco, S. M., & Starkey, W. L. 1954. A concept of fatigue damage. *ASME*, 76, 627–632.

McEvily, A. J. 1973. Phenomenological and microstructural aspects of fatigue. In: *Proceedings of the Third International Conference on the Strength of Metals and Alloys*.

Murakami, S. 1983. Notion of Continuum Damage Mechanics and its Application to Anisotropic Creep Damage Theory. *Journal of Engineering Materials and Technology, Transactions of the ASME,* 105, 99–105.

Murakami, S. 2012. *Continuum Damage Mechanics: A Continuum Mechanics Approach to the Analysis of Damage and Fracture.* Springer.

Needleman, A. 1990. An analysis of decohesion along an imperfect interface. *International Journal of Fracture*, 42, 21–40. 315

Newman, J. C. 1984. A crack opening stress equation for fatigue crack growth. *International Journal of Fracture*, 24, 131–135.

Paris, P. C., & Erdogan, F. 1963. A critical analysis of crack propagation laws. *Journal Of Basic Engineering*, 85(4), 528–534.

Peerlings, R. H. J. 1999. *Enhanced damage modelling for fracture and fatigue*. Ph.D. thesis, Technische Universiteit Eindhoven.

Peerlings, R. H. J., Brekelmans, W. A. M., Borst, R. de, & Geers, M. G. D. 2000. Gradient-enhanced damage modelling of high-cycle fatigue. *International Journal for Numerical Method in Engineering*, 49, 1547–1569.

Rabotnov, Y. N. 1968. Creep rupture. Pages 342–349 of: Hetenyi, M, & Vincenti, M (eds), *Proceedings of applied mechanics conference,* Springer, for Stanford University.

Roe, K. L., & Siegmund, T. 2003. An irreversible cohesive zone model for interface fatigue crack growth simulation. *Engineering Fracture Mechanics*, 70, 209–232.

Schütz, W. 1996. A history of fatigue. *Engineering Fracture Mechanics*, 54, 263–300.

Shet, C., & Chandra, N. 2002. Analysis of Energy Balance When Using Cohesive Zone Models to Simulate Fracture Processes. *Journal of Engineering Materials and Technology*, 124, 440–450.

Stanzl-Tschegg, S. E., & Mayer, H. 2001. Fatigue and fatigue crack growth of aluminium alloys at very high numbers of cycles. *International Journal of Fatigue*, 23, S231S237.

Ural, A., Krishnan, V. R., & Papoulia, K. D. 2009. A cohesive zone model for fatigue crack growth allowing for crack retardation. *International Journal of Solids and Structures*, 46, 2453–2462.

Walker, E. K. 1970. The effect of stress ratio during crack propagation and fatigue for 2024–T3 and 7076–T6 aluminum. In: *ASTM STP 462 Effect of environment and complex load history on fatigue life*. American Society for Testing and Materials.

Wang, B., & Siegmund, T. 2006. Simulation of fatigue crack growth at plastically mismatched bi-material interfaces. *International Journal of Plasticity*, 22, 1586–1609.

Wheeler, O. E. 1972. Spectrum Loading and Crack Growth. *Journal of Basic Engineering*, 94(1), 181–186. 316

Willenborg, J., Engle, R. M., & Wood, H. A. 1971. *A crack growth retardation model using an effective stress concept*. Tech. rept. Air Force Flight Dynamic Laboratory. Wright–Patterson Air Force Base, USA.

Wöhler, A. 1870. Über die Festigkeitsversuche mit Eisen und Stahl. *Zeitschrift für Bauwesen*, 20, 73–106.